Politecnico di Bari

Repository Istituzionale dei Prodotti della Ricerca del Politecnico di Bari

# Guided-Wave Optical Biosensors

This is a post print of the following article

*Original Citation:*
Guided-Wave Optical Biosensors / Passaro, V., Dell'Olio, F., Casamassima, B., DE LEONARDIS, F.. - In: SENSORS. - ISSN 1424-8220. - 7:4(2007), pp. 508-536. [10.3390/s7040508]

*Availability:*
This version is available at http://hdl.handle.net/11589/2401 since:

*Published version*
DOI:10.3390/s7040508

Publisher:

*Terms of use:*

(Article begins on next page)

26 June 2026

*Sensors* **2007**, *7*, 508-536

**sensors**

**ISSN 1424-8220**
© 2007 by MDPI
www.mdpi.org/sensors

*Review*

# Guided-Wave Optical Biosensors

**Vittorio M. N. Passaro [1,*], Francesco Dell'Olio [1], Biagio Casamassima [1] and Francesco De Leonardis [2]**

[1] Photonics Research Group, Dipartimento di Elettrotecnica ed Elettronica, Politecnico di Bari, via Edoardo Orabona n. 4, 70125 Bari, Italy

* E-mail: passaro@deemail.poliba.it; URL page: http://dee.poliba.it/photonicsgroup

[2] Photonics Research Group, Dipartimento di Ingegneria dell'Ambiente e per lo Sviluppo Sostenibile, Politecnico di Bari, viale del Turismo n. 8, 74100 Taranto, Italy

*Received: 23 March 2007 / Accepted: 24 April 2007 / Published: 25 April 2007*

---

**Abstract:** Guided-wave optical biosensors are reviewed in this paper. Advantages related to optical technologies are presented and integrated architectures are investigated in detail. Main classes of bio receptors and the most attractive optical transduction mechanisms are discussed. The possibility to use Mach-Zehnder and Young interferometers, microdisk and microring resonators, surface plasmon resonance, hollow and antiresonant waveguides, and Bragg gratings to realize very sensitive and selective, ultra-compact and fast biosensors is discussed. Finally, CMOS-compatible technologies are proved to be the most attractive for fabrication of guided-wave photonic biosensors.

**Keywords:** Biosensors, Surface Plasmon Resonance, Mach-Zehnder interferometers, Microdisk and Microring, Photonic technologies

---

## 1. Introduction

Photonic and electronic micro- and nano-sensors are emerging as very attractive devices to be employed in a great number of application fields such as medicine, microbiology, particle physics, automotive, environmental safety and defence.

In the last few years, a great effort has been devoted to sensor and actuator monolithic integration and micro-electro-mechanical system (MEMS) and micro-opto-electro-mechanical system (MOEMS) development. In the same period, optical sensors have attracted considerable attention because of their

immunity to electromagnetic interference, good compactness and robustness and high compatibility with fibre networks, but also because they usually exhibit shorter response time and higher sensitivities with respect to MEMS/MOEMS devices.

Sensors used for biochemical applications (e.g. biomolecules concentration measurement, DNA molecules investigation and pH estimation) must reach some specific performance requirements which are significantly different from those typical for other sensors. In particular, a biosensor has to be contextually highly sensitive and selective to the analyte being detected, to be biocompatible and immune to external disturbances as either pressure or temperature changes. Using photonic technologies, it is possible to fabricate very compact, highly performing and low cost biosensors.

A biosensor is a device which consists of a biologically or biophysically-derived sensing element (usually named *bio receptor*) integrated with a physical *transducer* that transforms a measurand into an output signal (Fig. 1).

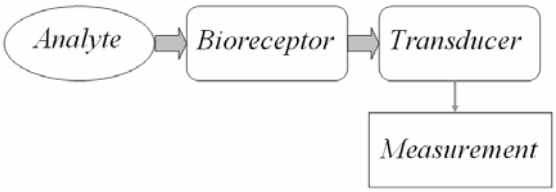


**Figure 1.** Operating principle of biochemical sensors.

As bio receptor, molecular species (antibody, enzyme, protein or nucleic acid) or a biological system (cells, tissue) are commonly employed to recognize biochemical substances. Transduction mechanisms are usually electrochemical, mass-based or optical. Electrochemical detection is commonly based on the chemical potential of particular species in solution (analytes) measured by comparison with a reference electrode. Mass-based detection exploits the change in oscillation frequency of a piezoelectric crystal which depends on applied electric signal frequency and crystal's mass.

In this paper we briefly review bio receptor classes and optical transduction mechanisms. Subsequently we investigate the wide spectrum of integrated photonic sensors proposed in literature, including those based on interferometer, hollow and antiresonant waveguides, employing Bragg gratings, adopting Surface Plasmon Resonance, and microcavities based on guided-wave sensors.

## 2. Bio receptors

A bio receptor is biological molecular specie or a biological system that adopts a biochemical mechanism for analyte recognition. The most used bio receptors are based on antibody-antigen, enzymatic, nucleic acid, or cellular interactions [1].

The antibodies (or immunoglobulin) are complex bio molecules formed by a hundred of amino acids arranged in a large Y-shaped ordered sequence (Fig. 2). The antibody recognizes a specific target, which is called antigen. An antibody contains two sites called *paratopes* that bind antigens. The interaction between an antibody and the relevant antigen is highly specific because their molecular

structures are complementary and antigen-antibody bond is very stable. Therefore antigen-antibody interaction is very rapid and antigen-antibody complex is characterized by a reasonable lifetime. Antigen-antibody reaction specificity enables to use antibodies as specific detectors capable to sense the analyte of interest even when its amount is very small and if a great number of other chemical substances are present in the sample.

In mammals there are five types of antibody: IgA, IgD, IgE, IgG, and IgM (where Ig stands for immunoglobulin). IgG provides the majority of antibody-based immunity against invading pathogens and it is the most useful in biochemical studies. IgG is composed of two subunits including two "heavy" chains and two "light" chains. These are assembled in a symmetrical structure and each IgG has two identical antigen recognition domains. The antigen recognition domain is a combination of amino acids relevant to both heavy and light chains. The molecule itself is roughly shaped like a Y and the regions of the Y extreme tips are the antigen recognition domains [1].

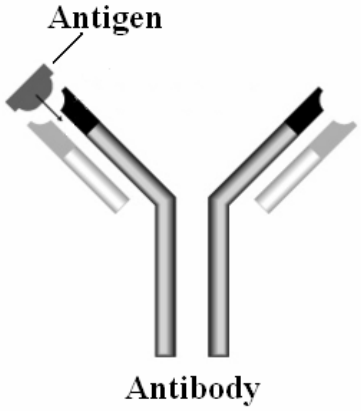


**Figure 2.** Interaction between antigen and antibody.

More attractive features for the employment of enzymes as bio receptors are their specific binding capabilities and their catalytic activity that permits to amplify the detection mechanism. Catalytic activity allows obtaining a lower detection limit in comparison with other techniques, but the catalytic activity is absent if the enzyme is denaturised (dissociated into its sub-unities or broken down in its component amino acids).

The DNA o RNA hybridization is often adopted as bio recognition mechanism exploiting the complementarities of the pairs of nucleotides: adenine (A)-thymine (T) and cytosine(C)-guanine (G). In particular, known DNA sequences (called *probes*) can be used to determine specific DNA sequences in biological samples. Finally, entire micro-organisms (as bacteria and fungi) can be used as bio receptors, for example, to test the toxicity of some substances.

## 3. Optical Transduction Mechanisms

### *3.1 Fluorescence*

Fluorescence phenomena are related to an energetic transition from an excited state to a lower energy level producing photon emission. Energy levels in an organic molecule are shown by the so called Jablonskii diagram (Fig. 3). In this diagram, $S_0$,…, $S_n$ and $T_1$,…, $T_m$ represent the discrete

electronic energy levels of a molecule ($S_1$,…, $S_n$ are excited singlet states and $T_1$,…, $T_m$ are excited triplet states). At equilibrium, molecules have the lowest possible energy $S_0$. When a molecule absorbs electromagnetic energy, it moves to an excited energy level (that usually is a singlet state). The energy level reached by the molecule absorbing electromagnetic energy depends on the incident radiation wavelength.

The intensity of the absorption (fraction of ground state molecules promoted to the electronic excited state) depends on the intensity of the excitation radiation (i.e., number of photons) and the probability of the transition with photons of the particular energy used. To characterize the intensity of an absorption band, a term often used is the oscillator strength *f*, which may be defined from the integrated absorption spectrum by the relationship [2]:

$$f = 4.315 \times 10^{-19} \cdot \int \varepsilon_v \cdot dv \tag{1}$$

where $\varepsilon_v$ is the molar extinction coefficient at the frequency $v$.

A molecule in an excited state tends to reach a lower energy level. Relaxation of the molecule from an excited state may occur in different manner. If relaxation takes place by emission of a photon without any change in spin multiplicity (from a singlet state to another singlet state), the transition is known as fluorescence. Emitted photon wavelength depends on loss energy by the molecule in the relaxation process.

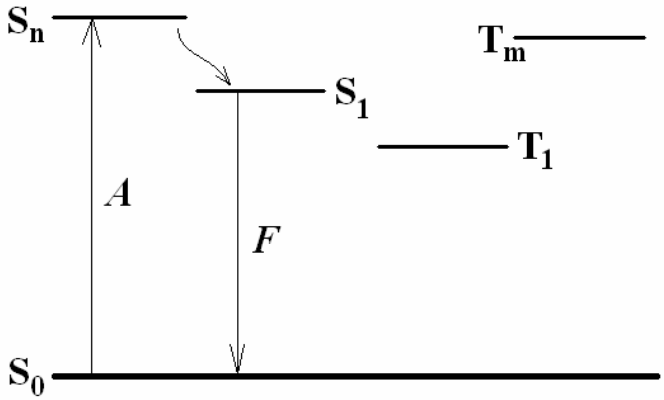


**Figure 3.** Jablonskii diagram.

The fluorescence quantum efficiency is defined as:

$$\phi_F = \frac{N^\circ_{L-P}}{N^\circ_{P-A}} \tag{2}$$

where $N^\circ_{L-P}$ is the number of luminescence photons, $N^\circ_{P-A}$ is the number of absorbed photons.

Fluorescence process can be characterized by its lifetime, defined as the time τ required for the emission to decrease to 1/e its original intensity, following a pulse excitation. Fluorescence lifetimes of organic molecules are of the order of $10^{-9}$ to $10^{-7}$ s.

Polarization is another physically observable property of the luminescence. It is caused by unique symmetries and orientations of electric moment vectors and wave functions involved in electronic transitions. The electric dipole moment determines the direction along which charge is displaced in a molecule undergoing an electronic transition. It is possible to study the polarization of the transition

using polarized light to excite and detect luminescence. Exciting the sample with polarized light and measuring the luminescence intensity along two perpendicular directions, it is possible to define the degree of polarization *P* as:

$$P = \frac{I_{EE} - I_{EB}}{I_{EE} + I_{EB}} \tag{3}$$

where $I_{EE}$ and $I_{EB}$ are luminescence intensities measured along the direction parallel and perpendicular to the excitation electric vector, respectively.

The degree of polarization is related to the angle $\eta$ between the absorption vector and the emission vector by the relation [2]:

$$P = \frac{3\cos^2 \eta - 1}{\cos^2 \eta + 3} \tag{4}$$

which is plotted in Fig. 4.

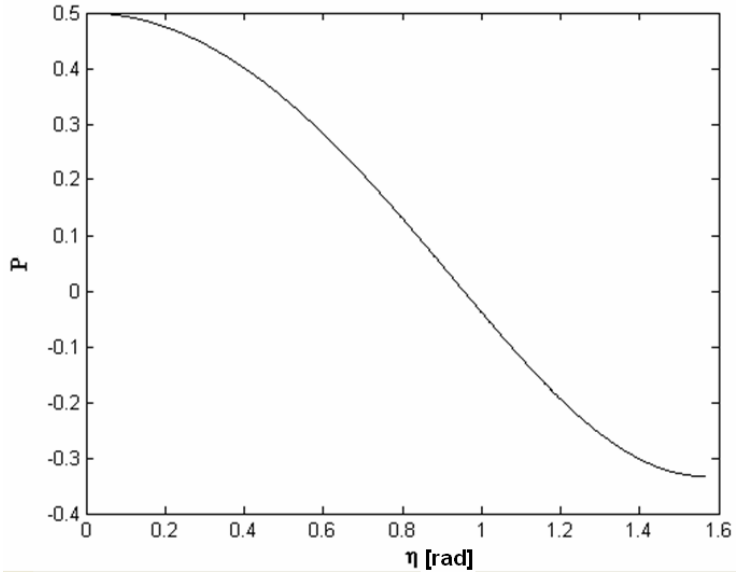


**Figure 4.** Degree of polarization versus $\eta$. If η = 0°, absorption and emission vectors are parallel and $P$ = 0.5. If η=90°, absorption and emission vectors are perpendicular and P = - 0.33.

The principle scheme of typical fluorescence-based biosensor is shown in Fig. 5. In this sensor, the optical signal provided by a laser propagates in an optical fibre until fibre section on which antibodies are immobilized. The optical radiation produced by antigen fluorescence is sent back to the detection system [3]. This sensor can be used to detect the carcinogen benzo[a]pyrene (BaP) or to distinguish BaP and benzopyrene tetrol (BPT) [4].

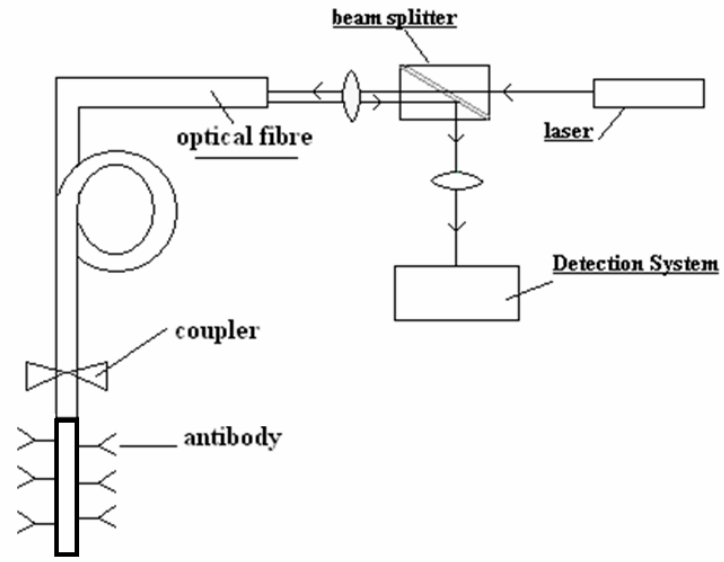


**Figure 5.** Typical fluorescence-based photonic sensor.

Fluorescence-based optical sensors are used in biochemical analyses of other chemical compounds and *in vivo* and *in vitro* analyses of tissues and cells (for example, neoplastic cells). Moreover, fluorescence is widely used in DNA sequencing (individuation of nucleotides sequence constituting DNA molecules), because it enables to reach a high readout speed [5].

### *3.2 Surface Plasmon Resonance*

Surface plasmon resonance is a charge-density oscillation that may exist at the interface between two media with dielectric constants of opposite signs, for instance a metal and a dielectric. The charge density wave is associated with an electromagnetic wave, whose field vectors reach its maximum at the interface and evanescently decays into both media. This surface plasma wave (SPW) is a TM-polarized wave (magnetic vector is perpendicular to SPW propagation direction and parallel to interface plane). When this wave interacts with a sample, SPW phase changes. Measuring this phase shift it is possible, for example, to investigate kinetics of the interaction between a protein and an antibody and to detect DNA hybridization [6-7].

### *3.3 Raman Scattering*

Raman spectroscopy is based on the Raman effect that results from energy exchange between incident photon and scattering molecules. In Rayleigh (or elastic) scattering, incident photon energy does not change after the collision and the scattered photon preserves the identical frequency as the incident photon. In Raman (or inelastic) scattering, energy is transferred from the molecule to the photon or vice versa. When the scattered photon has less energy than the incident photon, the process is referred to as Raman to Stokes scattering (Fig. 6 (a)). When the scattered photon has more energy than the incident photon, the process is known as Raman to anti-Stokes scattering (Fig. 6 (b)).

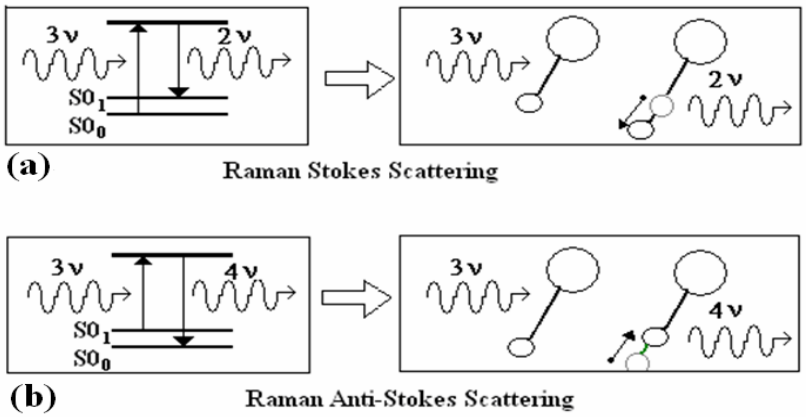


**Figure 6**. Raman scattering mechanisms.

Fig. 6 shows both Raman scattering mechanisms. In case of Raman to Stokes scattering, the molecule is at the lowest energetic level $S0_0$. When an electromagnetic beam strikes the sample, the molecule passes to a higher energetic level and then it returns to a lower energetic level $S0_1$ by emitting a photon. The difference between incident and emitted photon energy is used to change the vibration state of the molecule. In case of Raman to anti-Stokes scattering, the molecule initially is found at $S0_1$ level and, after that photonic beam has struck the sample, it reaches the $S0_0$ level with a photon emission.

Raman signals are usually weak and require powerful sources and sensitive detectors. Only a limited number of biological molecules contribute to tissues fluorescence whereas most biological molecules are Raman active, so Raman spectroscopy can overcome some limitations of fluorescence, for example, in cancer diagnosis.

Fig. 7 shows a typical apparatus used in Raman spectroscopy. It consists of a laser that provides optical signal used to produce Raman effect, a fibre that collects optical signals exiting from the sample, and a spectrograph connected to a processing unit [8]. Raman spectroscopy has been used for human immunodeficiency virus (HIV) detection [9] and in DNA fragments sequencing [10].

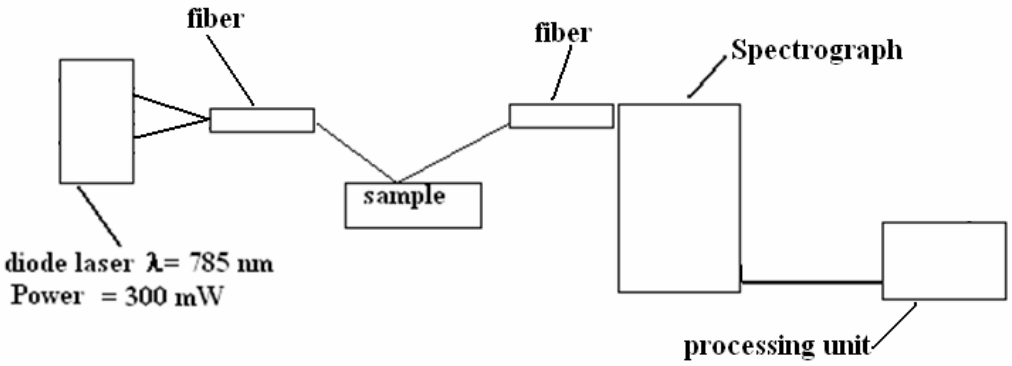


**Figure 7.** Typical apparatus for Raman spectroscopy.

*3.4 Absorption change*

Lambert-Beer law relates a solution absorbance $A$ to an analyte dispersed in this solution concentration $C$ by the following relation:

$$A = \varepsilon LC \tag{5}$$

where $L$ is the optical path length and $\varepsilon$ is the wavelength-dependent molar absorption coefficient. Measuring the solution absorbance, it is possible to estimate some bio analyte concentration in aqueous solutions. This transduction mechanism is used in some integrated optical and optical fibre biosensors to sense biological pathogens or gases (as oxygen or carbon dioxide) concentrations and to measure pH in solutions [11].

*3.5 Photon migration spectroscopy*

The photon migration spectroscopy is a technique that combines experimental measurements and model-based data analysis to measure the bulk absorption properties of highly scattering media. The photons diffusively propagate throughout the tissue, in random direction. Due to this technique, it is possible to obtain information about tissue structure and function [12].

The transport theory is a statistical bookkeeping scheme that treats photons as no interacting point-particles undergoing elastic interactions. The quantity of interest is the photon density $U(\vec{r},t)$. Transport equation is easy to assemble, but difficult to solve analytically. The so-called $P_1$ approximation keeps only first order spherical harmonic expansion terms of the transport equation.

Assuming an isotropic point source and adopting $P_1$ approximation, the equation of the photon density $U(\vec{r},t)$ in terms of the optical properties of the tissue [1] is:

$$\nu D\left[\frac{3}{\nu^2}\frac{\partial^2 U(\vec{r},t)}{\partial t^2} - \nabla^2 U(\vec{r},t)\right] + (1+3\mu_a D)\frac{\partial U(\vec{r},t)}{\partial t} + \nu\mu_a U(\vec{r},t) = Q(\vec{r},t) + \frac{3D}{\nu}\frac{\partial Q(\vec{r},t)}{\partial t} \tag{6}$$

where $\nu$ is the light speed inside the medium, $\nu D = \nu\left(3\cdot(\mu_a+\mu_s)\right)^{-1}$ is the optical diffusion coefficient, $Q(\vec{r},t)$ is the photonic density per unit time injected by the source, and $\mu_{s,a}$ are scattering ($s$) and absorption ($a$) lengths. Assuming a macroscopically homogeneous medium and supposing to be far from sources and boundaries and $\mu_s >> \mu_a$, we have:

$$Q(\vec{r},\omega,t) = S(\omega)\cdot\exp\left(j\cdot(\omega\cdot t + \phi_0(\omega))\right)\cdot\delta(\vec{r}) \tag{7}$$

where $S(\omega)$ and $\phi_0(\omega)$ are frequency-dependent instrumental factors called source strength and source phase, respectively.

Assuming that $U(\vec{r},t,\omega) = U(\vec{r},\omega)\cdot\exp(.j\cdot\varpi\cdot t)$ and replacing Eq. (7) into Eq. (6), we can write Eq. (6) in the following form:

$$\left[\nabla^2 - k^2(\omega)\right]U(\vec{r},\omega) = -\frac{S(\omega)}{\nu D}e^{-j\phi_0(\omega)}\delta(\vec{r}) \tag{8}$$

where

$$k^2(\omega) = \frac{\mu_a}{D} \cdot \left[ 1 - j \frac{\omega}{\mu_a \cdot \nu} (1 + 3\mu_a \cdot D) \right] \tag{9}$$

The obtained equation (Eq. (8)) is a Helmholtz equation which admits the following solution if infinite-medium boundary conditions ($U \to 0$ if $r \to \infty$) are imposed:

$$U(\bar{r}, \omega) = \frac{S(\omega)}{4\pi \cdot \nu \cdot D \cdot r} \exp(-j \cdot \phi_0(\omega) + k(\omega) \cdot r) \tag{10}$$

Assuming $\mu_a = 0.006\ mm^{-1}$ and $\mu_s = 1.0\ mm^{-1}$, $k$ real and imaginary part dependence on $f = \omega/2\pi$ has been calculated by Eq. (9) (see Fig. 8).

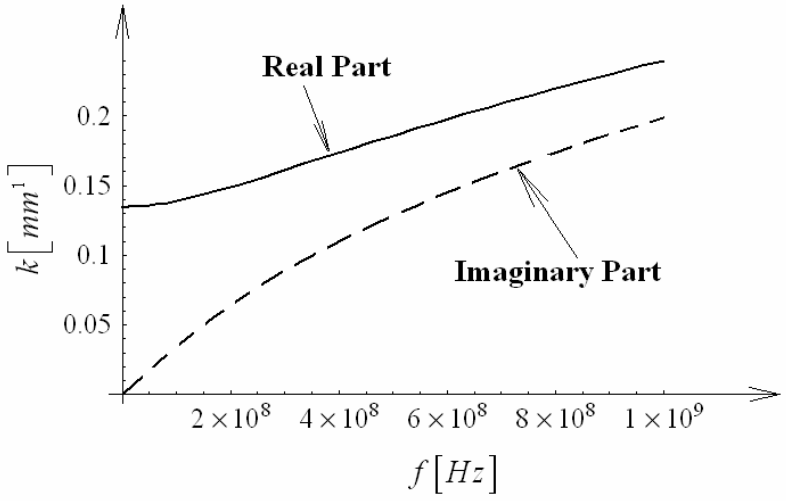


**Figure 8.** Real and imaginary parts of the wave vector, *k*, assuming $\mu_a = 0.006\ mm^{-1}$ and $\mu_s = 1.0\ mm^{-1}$.

*3.6 Effective index change in guiding structures*

In an optical guiding structure a shift of propagating optical mode effective index can be induced by two different physical phenomena (see Fig. 9):

*i)* the change of thickness (equal to $\rho$) of an adlayer constituted by adsorbed or bound molecules which are transported (by convection or diffusion) from the gaseous or liquid medium, that serves as waveguide cover medium, to cover medium/guiding film interface;

*ii)* the change of refractive index $n_c$ of the homogeneous liquid that serves as waveguide cover medium.

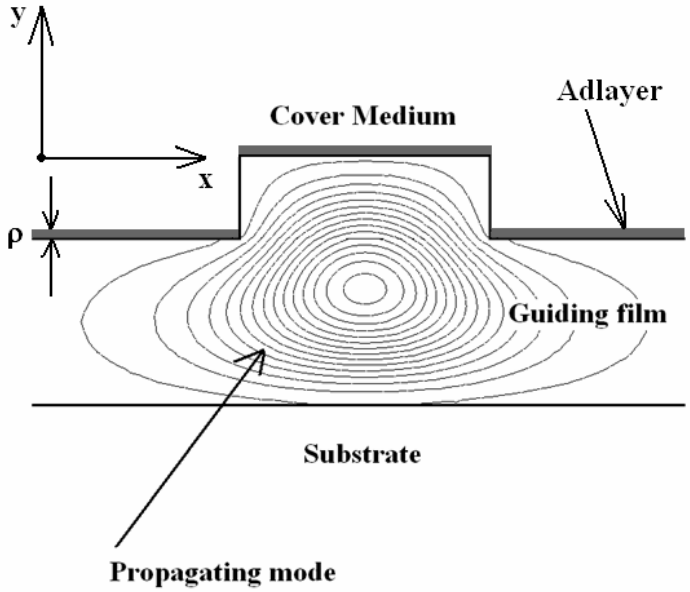


**Figure 9**. Effective index change in integrated optical sensors.

In case of a change in $n_c$, we can write:

$$\Delta n_{eff} = \frac{2\Delta n_c \, n_c^0}{\eta_0 P} \iint_C \left|\mathbf{E}(x,y)\right|^2 dxdy = \frac{2n_c^0 \Delta n_c \Gamma_C}{\eta_0 P} \iint_\infty \left|\mathbf{E}(x,y)\right|^2 dxdy \tag{11}$$

where

$$P = \iint_\infty \left[\left(\mathbf{E}\times\mathbf{H}^* + \mathbf{E}^*\times\mathbf{H}\right)\bullet\hat{z}\right]dxdy \tag{12}$$

$\Delta n_{eff}$ is the shift in effective index produced by change in cover medium refractive index $\Delta n_c$, $\eta_0$ is impedance of free space, **E** and **H** are electric and magnetic field vectors, $\hat{z}$ indicates the unit vector along $z$ direction (propagation direction), $C$ indicates cover medium region, $\Gamma_C$ is the confinement factor in cover medium and $n_c^0$ is the unperturbed value of cover medium refractive index.

If a change of $\rho$ is induced by the analyte, $\Delta n_{eff}$ is given by:

$$\Delta n_{eff} = \frac{n_{ml}^2 - \left(n_c^0\right)^2}{\eta_0 P} \iint_M \left|\mathbf{E}(x,y)\right|^2 dxdy \tag{13}$$

where $n_{ml}$ is molecular adlayer refractive index and $M$ is the region in which the adlayer thickness increase takes place.

## 4. Integrated optical biosensors

Integrated optical sensors adopt a waveguide to confine optical power and are based on evanescent field sensing. Although light is confined within the guiding film of the waveguide, there is a part of the guided light that travels through a region extending outside, into the medium surrounding the waveguide, and can interact with the environment. This kind of optical sensors exhibits very interesting advantages with respect to other optical sensors, such as compactness, very high sensitivity and possibility of mass production.

In a large number of integrated optical biosensors proposed in the last few years, the analyte presence either produces a shift in waveguide cover medium refractive index (*homogeneous sensing*), or determines the thickness increase of a molecular layer deposited on guiding film/cover medium interface (*surface sensing*). Both phenomena affect the propagating optical mode effective index which is measured in different ways, according with specific biosensor architecture.

*4.1 Interferometer architectures*

Interaction between the sample and the optical signal propagating in the sensor produces a change of optical mode effective index and, then, in its phase. To convert this phase shift in an amplitude change, interferometer architectures are commonly used. Among these architectures, Mach-Zehnder approach assures a very high sensitivity and is largely most used. In this kind of integrated optical biosensors (see Fig. 10); input optical signal is split by a Y-junction in two signals. These two signals propagate in the reference and sensing arms (in this last arm the interaction between the sample and the optical signal takes place). After the propagation in these two arms, the two optical signals accumulate a phase shift $\Delta\varphi$. Phase shifted optical signals interfere by an output Y-branch.

If input power $P_{in}$ is unequally divided by input Y-junction between the two arms (the sensing arm receives an optical power equal to $\gamma_1 \cdot P_{in}$ and the reference arm receives an optical power equal to $(1-\gamma_1)\cdot P_{in}$) and output power coming from output Y-junction is the sum of optical power coming from sensing arm multiplied by $\gamma_2$ and optical power coming from reference arm multiplied by $(1-\gamma_2)$ (see Fig. 10), the ratio between the output and input powers is given by:

$$\frac{P_{out}}{P_{in}} = \gamma_1\gamma_2 + (1-\gamma_1)\cdot(1-\gamma_2) + 2\sqrt{\gamma_1\gamma_2(1-\gamma_1)(1-\gamma_2)}\cdot cos(\Delta\varphi) \tag{14}$$

where

$$\Delta\varphi = 2\pi\frac{L}{\lambda}\left(n_{eff}^{S} - n_{eff}^{R}\right) \tag{15}$$

$L$ is the reference and sensing arm length, $\lambda$ is the optical signal wavelength, $n_{eff}^{S}$ is the effective index of mode propagating in sensing arm and $n_{eff}^{R}$ is the effective index of mode propagating in reference arm.

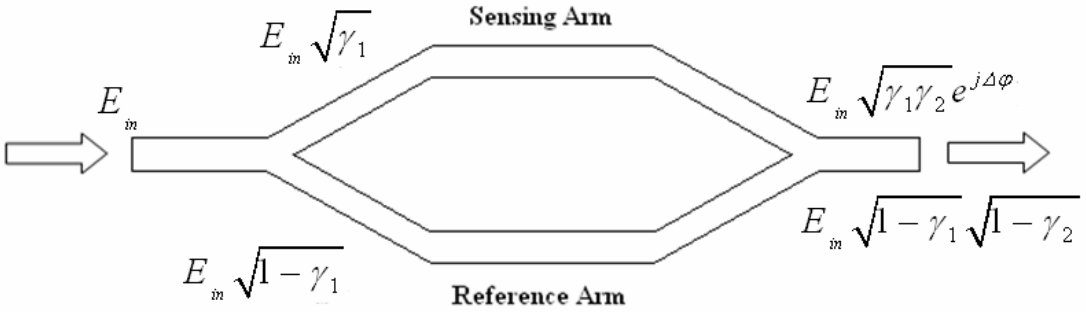


**Figure 10**. Mach-Zehnder interferometer architecture.

Fig. 11 shows the contour plot of $\frac{P_{out}}{P_{in}}$ ratio (for $\Delta\varphi = 0$) with respect to $\gamma_1$ and $\gamma_2$. We observe that $\frac{P_{out}}{P_{in}} = 1$ if $\gamma_1 = \gamma_2$. The perfect matching is obtained for $\gamma_1 = \gamma_2 = \frac{1}{2}$. In fact, as it is shown in Fig. 12, only when $\gamma_1 = \gamma_2 = \frac{1}{2}$ the sensor exhibits maximum extinction ratio (ratio between $\frac{P_{out}}{P_{in}}$ value when $\Delta\varphi = 0$ and $\frac{P_{out}}{P_{in}}$ value when $\Delta\varphi = \pi$).

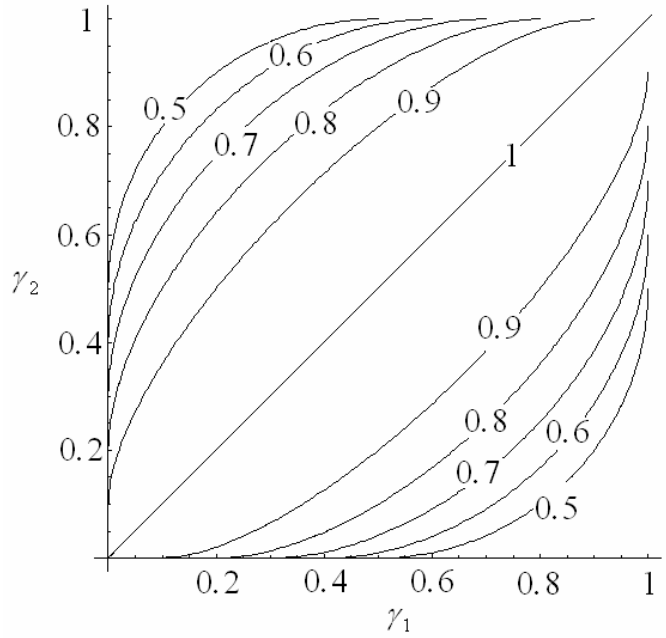


**Figure 11.** Contour plot of output/input power ratio ($P_{out}/P_{in}$) versus $\gamma_1$ and $\gamma_2$.

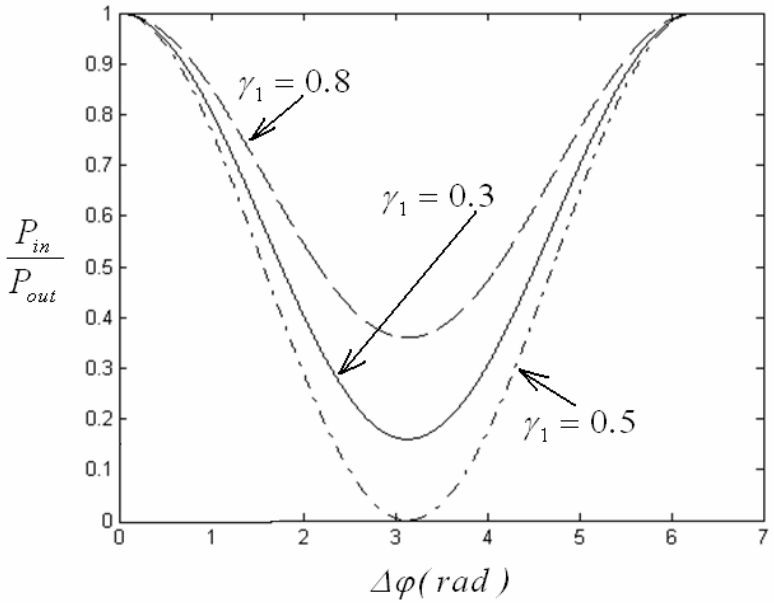


**Figure 12.** Output/input power ratio versus $\Delta\varphi$ for different $\gamma_1$ values (we assume $\gamma_1 = \gamma_2$).

In the last two decades, a great number of integrated optical sensors based on Mach-Zehnder interferometers (MZI) have been realized to detect different chemical species as organic compounds [13-14] and proteins [15-17]. Technologies employed for fabrication of these sensors are prevalently CMOS-compatible (guiding film in silicon, silicon nitride or silicon oxynitride) but glasses [18-19] and III-V semiconductor compounds [20] technologies have been also proposed.

The sensitivity $S$ of sensors based on Mach-Zehnder interferometer can be expressed, assuming that $\Delta\varphi$ varies in a narrow range around $\pi/2$, as:

$$S = -\frac{2\pi}{\lambda} L S_w \tag{16}$$

where $S_w$ is the waveguide sensitivity, defined in case of homogeneous sensing, as:

$$S_w = \frac{\partial n_{eff}}{\partial n_C} \tag{17}$$

and, in case of surface sensing, as:

$$S_w = \frac{\partial n_{eff}}{\partial \rho} \tag{18}$$

where $n_{eff}$ is the effective index of optical mode propagating in guiding structure, $n_c$ is the cover medium refractive index and $\rho$ is the thickness of molecular layer deposited on guiding film/cover medium interface. Moreover, sensitivity of integrated optical sensors adopting Mach-Zehnder architecture depends on sensing arm length $L$, so it is limited only by the undesired shift in propagating mode effective index (due to, for example, any temperature change). Thus, a trade-off between device length and device sensitivity has to be usually achieved.

In [21] a Mach-Zehnder optical biosensor has been fabricated, capable to monitor antigen-antibody immunoreactions, having a detection limit in terms of minimum detectable change in cover medium refractive index equal to $7\times10^{-6}$. A detection limit equal to $1.5\times10^{-6}$ has been obtained by a Mach-Zehnder optical biosensor fabricated using a waveguide produced in a BGG36 glass substrate [22].

In glass based MZI, a graded index waveguide is commonly adopted. This kind of guiding structure supports optical modes having a week evanescent field and so exhibits a reduced sensitivity. To improve glass waveguide sensitivity, in [23], the adoption of a channel-planar composite optical waveguide (COWG) to realize MZI sensing arm has been proposed. As shown in Fig. 13, a channel-planar COWG consists of a single-mode channel waveguide locally overlaid with a tapered film. This kind of guiding structure permits to enhance evanescent field and consequently waveguide sensitivity.

Other configurations adopted for interferometer integrated optical biosensors are those based on Young interferometers. Using a four-channel Young interferometer, the simultaneous and independent monitoring of tree antigen-antibody reactions has been achieved [24]. In this device the generated interference pattern is recorded by a CCD camera and analyzed by Fast Fourier Transform (FFT) algorithm. In this manner a detection limit of $8.5 \times 10^{-8}$ has been obtained.

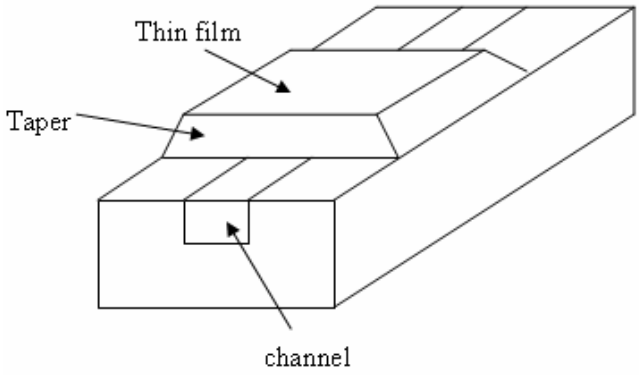


**Figure 13.** Schematic diagram of a channel-planar composite optical waveguide.

*4.2 Architectures based on anti-resonant reflecting optical waveguides*

Anti-resonant reflecting optical waveguide (ARROW) is a five-layer guiding structure where light is confined within the core layer by total internal reflection at the cover medium/core interface and by anti-resonant reflection (reflectivity of around 99.96%) due to the presence of the two cladding layers underneath the core, as it is shown in Fig. 14.

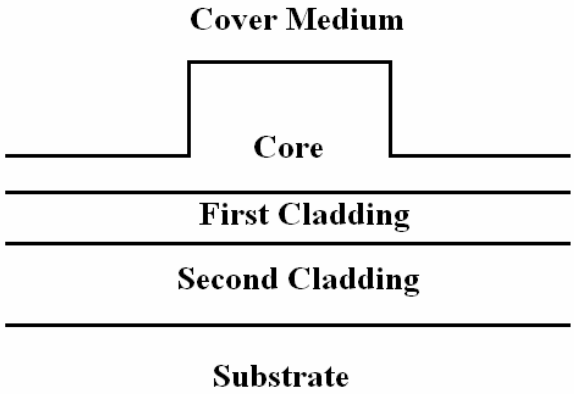


**Figure 14.** ARROW waveguide structure.

ARROW is a leaky guiding structure with virtual mono-mode behaviour, where higher order modes are filtered out by loss discrimination due to the low reflectivity assured to these modes by the two cladding layers. The refractive indices and thicknesses of the cladding layers have to be properly designed for the working wavelength to assure high reflectivity and, therefore, good guiding characteristics. ARROWs are usually fabricated in a CMOS-compatible technology and the materials commonly used are silicon for the substrate, silicon oxide for the core and second cladding layers and silicon nitride for the first cladding.

ARROW structures exhibit low losses, permit larger dimensions than conventional total internal reflection-based waveguides (micrometers instead of nanometers), enable to confine optical power in low index material (as silicon oxide) and exhibit a good sensitivity. These features is quite attractive for sensing applications, so ARROWs employment in highly sensitive and low cost integrated optical

sensors has been discussed [25-27]. In [28] a Mach-Zehnder interferometer adopting an ARROW as guiding structure has been used to fabricate a 15 mm long optical biosensor having a detection limit of $2\times10^{-5}$.

*4.3 Architectures based on hollow waveguides*

Hollow waveguides permit to simultaneously confine the optical power and the solution to be analyzed in the waveguide core constituted by a low-index liquid substance. In this kind of waveguides, the optical signal is confined inside the core (whose refractive index is around 1.33) by two cladding layers designed to produce the anti-resonant reflection (see Fig. 15).

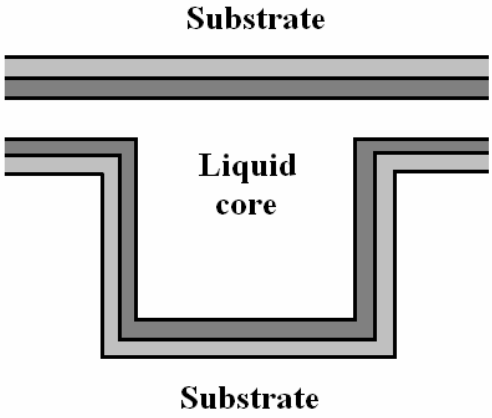


**Figure 15.** Hollow waveguides cross section.

In [29] a liquid core hollow waveguide has been adopted to realize an integrated sensor capable to detect refractive index changes in liquid substance constituting the core. This sensor exhibits a minimum detectable change in core medium refractive index equal to $9\times10^{-4}$.

*4.4 Architectures based on surface plasmon resonance*

Integrated optical biosensors exploiting surface plasmon resonance (SPR) are constituted by a single mode waveguide produced, for example, by thermal ion-exchange in a glass substrate. A small region of the waveguide is coated with a thin metal film. This metal-coated part of the sensor can support a SPW and forms the interaction region with the solution containing the analyte. The structure incorporates a Y-junction used as 3 dB power splitter. A quasi-TM mode is excited in the input waveguide. After passing through the 3 dB power divider, this mode couples across the step discontinuity between the metal coated and uncoated waveguide regions exciting the surface plasmon wave (SPW). After propagating through the metal-coated region of the sensor, SPW excites the optical mode in the uncoated output waveguide (see Fig. 16).

In [30] an integrated optical biosensor for simazine detection has been designed and fabricated. This sensor exhibits a minimum detection of $1\times10^{-4}$ and a detection limit equal to 0.1 μg/l for simazine concentration measurements. A minimum detectable change in cover medium refractive index equal to $1.2\times10^{-6}$ is achievable by the SPR based integrated biosensor proposed in [31]. This sensor is able to detect 2 nm of human chorigonadotropin present in 1 ml of 1% bovine serum albumin solution.

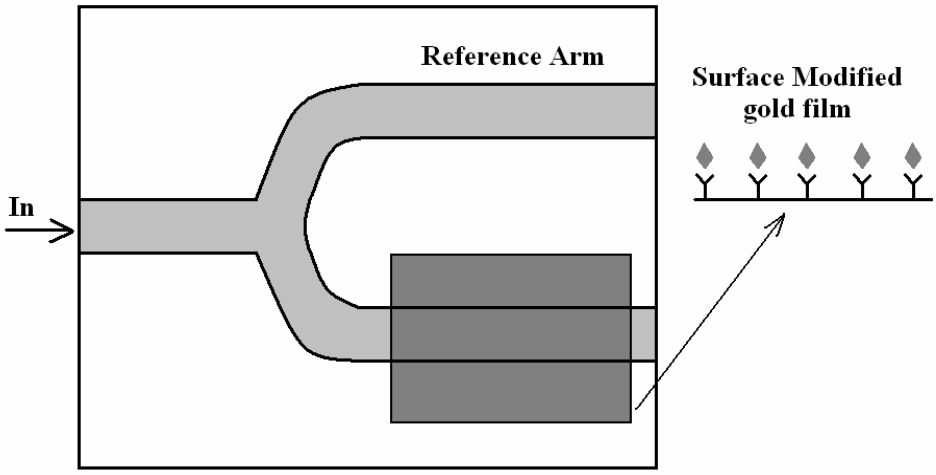


**Figure 16.** Integrated optical biosensor exploiting the SPR scheme.

Assuming a planar structure as that shown in Fig. 17, the propagation constant of a SPW propagating at the interface between a metal and a dielectric medium is given by [32]:

$$k_{SPW} = k_0 \cdot \sqrt{\frac{\varepsilon_m \cdot n_d^2}{\varepsilon_m + n_d^2}} \tag{19}$$

where

$$k_0 = \frac{2\pi}{\lambda} \tag{20}$$

$\lambda$ is the free space wavelength, $\varepsilon_m$ is the dielectric constant of the metal, and $n_d$ is the refractive index of the dielectric medium. The dielectric constant of the metal $\varepsilon_m$ is complex so SPW propagation constant is complex too. If imaginary part of $\varepsilon_m$ can be neglected, real part of $k_{SPW}$ can be written as:

$$\Re\{k_{SPW}\} = k_0 \cdot \sqrt{\frac{\Re\{\varepsilon_m\} \cdot n_d^2}{\Re\{\varepsilon_m\} + n_d^2}} \tag{21}$$

where $\Re$ indicates the real-part operator. The real part of the SPW propagation constant $\Re\{k_{SPW}\}$ is always larger than that of an optical wave propagating in the dielectric medium so direct coupling between optical wave and SPW is not possible. In order to optically excite the SPW, the propagation constant of light in the dielectric medium has to be increased. This enhancement can be done using either attenuated total reflection (ATR) method or grating couplers.

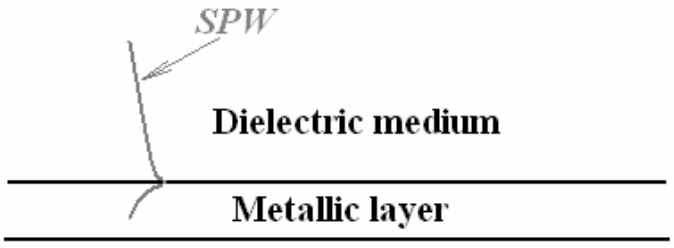


**Figure 17.** Planar structure in which SPW propagates.

*4.7 Architectures based on Bragg gratings*

It is well known that a Bragg grating is a 3D periodic structure (Fig. 18) whose refractive index profile can be expressed as:

$$n(x, y, z) = n_0(x, y) + \Delta n(x, y, z) \tag{22}$$

where $n_0(x,y)$ is the waveguide index distribution and $\Delta n(x,y,z)$ is the periodic refractive index perturbation whose period $\Lambda$ along $z$ has to satisfy the following relation:

$$\Lambda = \frac{m}{2n_{eff}}\lambda_c \tag{23}$$

where $m$ is the grating order, $\lambda_c$ is the centre wavelength of the spectral response and $n_{eff}$ is the effective index of the propagating mode. From Eq. (23) it is evident that a change in refractive index of guiding structure cover medium (and consequently in the propagating mode effective index), produces a centre wavelength shift of grating reflection and transmission spectra. This shift permits to measure biochemical quantities that affect the cover medium refractive index.

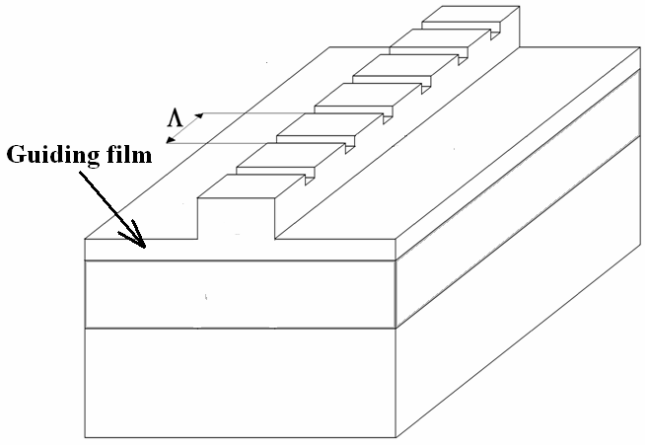


**Figure 18.** Bragg grating structure.

The use of Bragg gratings as building blocks for fabrication of highly sensitive and very compact integrated optical biosensors has been proposed in [33-34]. A 76 μm long first order Bragg grating has been fabricated using a $Si_3N_4/SiO_2$ waveguide and minimum detectable change in refractive index cover medium has been calculated as equal to $4\times10^{-5}$ [34]. Bragg grating based sensitivity is given by:

$$S \triangleq \frac{\partial \lambda_c}{\partial n_C} = S_w \frac{\lambda_c}{2n_{eff}} \tag{24}$$

where $n_C$ is the cover medium refractive index and $S_w$ is the waveguide sensitivity whose definition depends on sensing mechanism (homogeneous or surface sensing).

Using sub-micrometer silicon-wire waveguides (see Fig. 19) realized by Silicon-on-Insulator (SOI) technological platform as guiding structure, a very high $S_w$ is obtainable (a value of 0.31 has been experimentally proved in [35]). Because for optical modes propagating in Si-wire waveguides effective indices are around 2 and $\lambda_c$ can be fixed as equal to 1550 nm, a device sensitivity $S$ around 120 nm is practically obtainable.

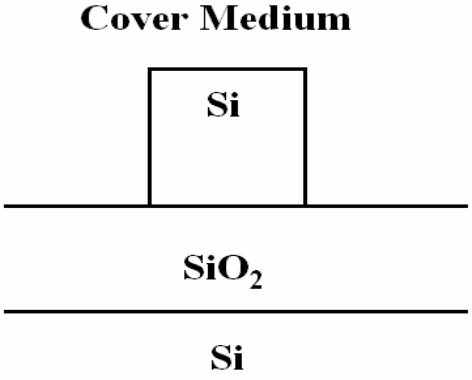


**Figure 19.** Si-wire waveguide structure.

*4.8 Architectures based on silicon slot waveguides*

Recently, sub-micrometer slot waveguides realized by using SOI technology (Fig. 20) are emerging as very attractive guiding structures for integrated optics [36]. This kind of guiding structure is constituted by two Si-wires very close to each other and supports a quasi-TE mode highly confined in the low index gap region between the two Si-wires (see Fig. 21).

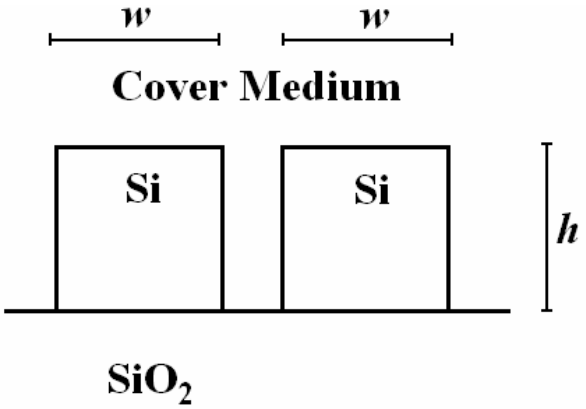


**Figure 20.** SOI slot waveguide structure.

In last two years, a great variety of optical devices has been realized adopting slot waveguides, including micro-ring resonators, optical modulators, electrically pumped light emitting devices,

directional couplers, all-optical logic gates and beam splitters. High values (around 65%) reached by confinement factor in cover medium $\Gamma_C$ when quasi-TE modes propagates in a slot waveguide, suggest to adopt this guiding structure for ultra-compact and ultra-sensitive integrated optical biosensor fabrication (see Eq. 11, showing the waveguide sensitivity $S_w$ as proportionally depends on $\Gamma_C$). Recently, a Finite Element Method (FEM)-based investigation of silicon slot waveguide sensitivity has demonstrated that this guiding structure can exhibit sensitivity values significantly larger than those shown by other very sensitive waveguides (such as Si-wire waveguides) [37].

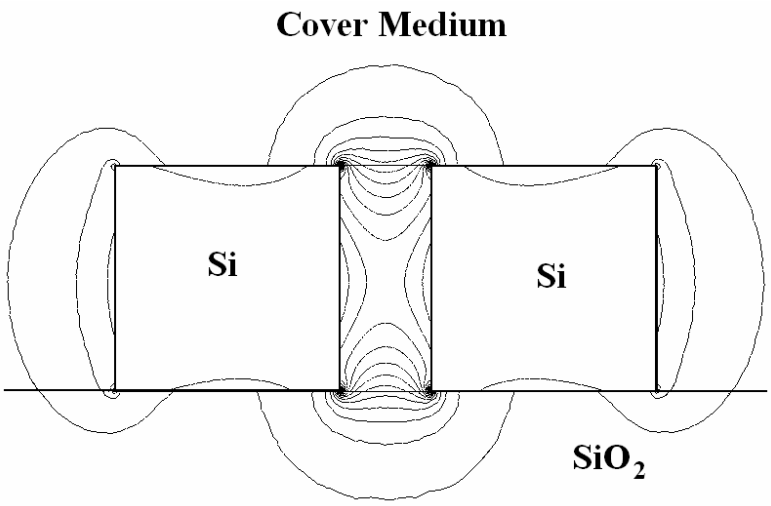


**Figure 21.** Quasi-TE mode profile in silicon slot waveguide.

*4.9 Architectures based on integrated optical micro cavities*

Microring and micro-racetrack resonators are emerging as very attractive building-blocks for micrometer-scale photonics, essentially because of their compactness and versatility. In fact, a great number of optical functions related to telecommunications systems such as filtering, modulation, amplification and switching can be performed using guided-wave micro-resonators. The use of optical micro-resonators in sensing applications is a relatively new research field.

Micro-resonator advantages in sensing applications are related to the device size reduction by some orders of magnitude which do not compromise the device sensitivity, because the large photon lifetime within the resonator at the resonance provides an equivalently long interaction length to achieve a detectable phase shift.

Light coupled to micro resonators is confined within the structure by total internal reflection forming high quality factor resonant modes. Any interaction with the evanescent tail of the optical field (usually the change in waveguide cover medium refractive index) affects the guided mode, and thus changes the resonance behaviour of the cavity (Fig. 22). This change in resonance can be detected with very high sensitivity by optimizing the micro cavity design and the method of observation.

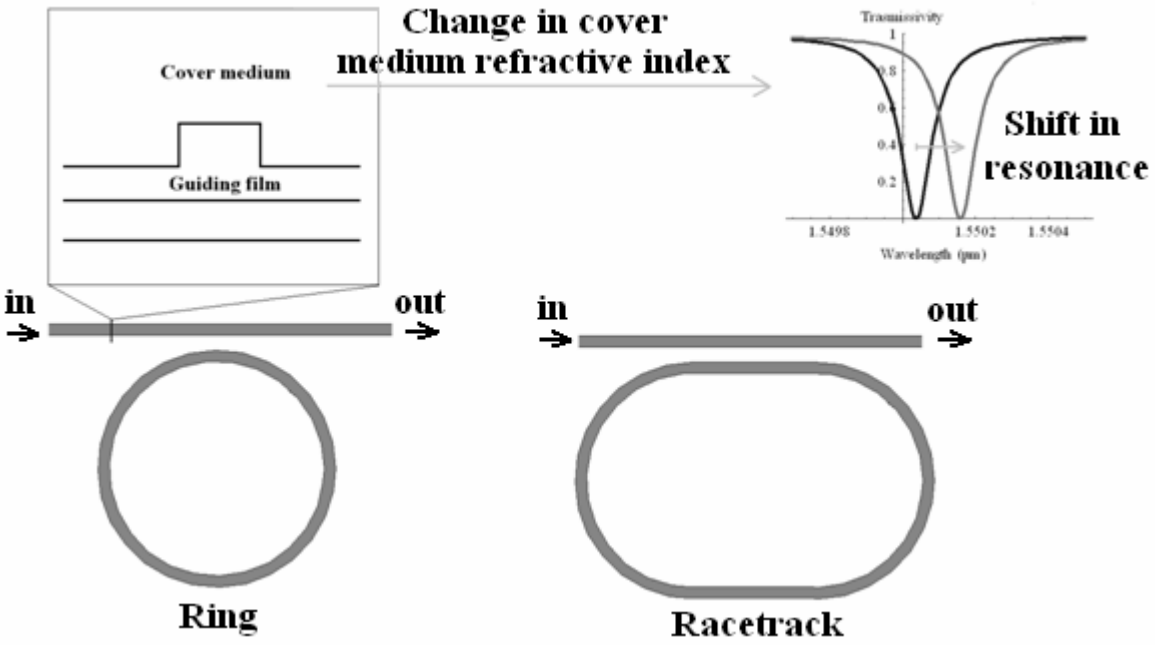


**Figure 22.** Micro cavity-based architectures for integrated optical sensors.

Any micro-racetrack resonator can be theoretically investigated by using the schematic diagram in Fig. 23 (microring resonator can be seen as a micro-racetrack resonator in which the resonator straight section has a length $L_S$ equal to zero, and so it can be described adopting the same formalism).

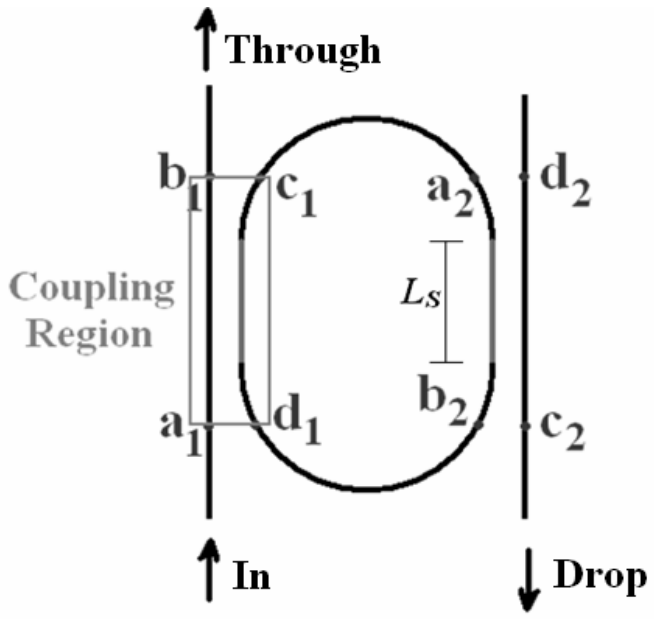


**Figure 23.** Resonator race-track structure schematic representation.

The electromagnetic interactions in the coupling regions can be described using the following matrices [38]:

$$\begin{bmatrix} b_k \\ c_k \end{bmatrix} = \begin{bmatrix} r & it \\ it & r \end{bmatrix} e^{i\beta L_c} \begin{bmatrix} a_k \\ d_k \end{bmatrix} \qquad (k = 1,2) \tag{25}$$

where $a_k$, $b_k$, $c_k$, $d_k$ ($k$ = 1,2) are the output and the input electric fields in the coupling regions (Fig. 23), $L_c$ is the total optical path length in the coupling region, $r$ and $t$ are self and cross coupling coefficients and $\beta$ is the propagation constant of optical mode propagating in the micro cavity.

Optical propagation in the resonator portion outside coupling region can be modelled by following relations [38]:

$$a_2 = c_1\sqrt{A}e^{i\beta\frac{L_p}{2}} \tag{26}$$

$$d_1 = b_2\sqrt{A}e^{i\beta\frac{L_p}{2}} \tag{27}$$

where $L_p$ is the optical path length that light travels inside the racetrack except for the coupling region and $A$ is the optical field loss factor resulting from the light propagating over $L_p$.
Supposing that:

$$d_2 = 0 \tag{28}$$

we obtain:

$$b_1 = r\frac{1-\left(r^2+t^2\right)Ae^{i\beta L}}{1-r^2Ae^{i\beta L}}e^{i\beta L_c}a_1 \tag{29}$$

$$c_2 = \frac{-t^2\sqrt{a}e^{i\beta\left(\frac{L_p}{2}+L_c\right)}}{1-r^2Ae^{i\beta L}}e^{i\beta L_c}a_1\,. \tag{30}$$

Rearranging Eq. (29) and Eq. (30), it is possible to calculate optical power exiting from resonator through and drop ports (see Fig. 23). These two quantities, indicated as $T$ and $D$, are equal to:

$$T = \left|\frac{b_1}{a_1}\right|^2 = r^2\left|\frac{1-\left(r^2+t^2\right)Ae^{i\delta}}{1-r^2Ae^{i\delta}}\right|^2 \tag{31}$$

$$D = \left|\frac{c_2}{a_1}\right|^2 = \frac{At^4}{\left|1-r^2Ae^{i\delta}\right|^2} \tag{32}$$

where $\delta = \beta\cdot(2L_c+L_p)$.

Transmittivity $T$ assumes its minimum values for $\delta=2q\pi$ ($q$ is an integer number) ant it is maximum for $\delta=(2q+1)\pi$. Maximum and minimum transmittivity values are given by:

$$T_{max} = r^2\left|\frac{1+\left(r^2+t^2\right)A}{1+r^2A}\right|^2 \tag{33}$$

$$T_{min} = r^2\left|\frac{1-\left(r^2+t^2\right)A}{1-r^2A}\right|^2 \tag{34}$$

Optical power at drop port is maximum for $\delta=2q\pi$ and minimum for $\delta=(2q+1)\pi$. Maximum and minimum $D$ values can be written as:

$$D_{max} = \frac{At^4}{\left|1 - r^2 A\right|^2} \tag{35}$$

$$D_{min} = \frac{At^4}{\left|1 + r^2 A\right|^2} \tag{36}$$

Under resonance condition (minimum transmittivity), we have that:

$$\delta = 2q\pi \;\Rightarrow\; \beta L = 2q\pi \;\Rightarrow\; \frac{2\pi}{\lambda} n_{eff} L_t = 2q\pi \tag{37}$$

where $n_{eff}$ is optical mode propagating in the resonator effective index and $L_t = 2L_c+L_p$. Resonance wavelengths are given by:

$$\lambda_{res} = \frac{n_{eff} L}{q}. \tag{38}$$

Two very important parameters of micro resonator performance are quality factor $Q$ and finesse $F$. They are defined as:

$$Q = \frac{\lambda_{res}}{\Delta\lambda} \tag{39}$$

$$F = \frac{\Delta\lambda}{\delta\lambda} \tag{40}$$

where $\Delta\lambda$ is the difference between two adjacent resonance wavelengths and $\delta\lambda$ is the full-width-at-half-maximum (FWHM) of the considered resonance wavelength (see Fig. 24).

Assuming an optical resonator having $L_t$ = 100 μm, $A$=0.99, $r^2$=0.7, $t^2$=0.3 and $n_{eff}$=2, and using Eq. (31), the transmittivity spectrum reported in Fig. 25 has been calculated. If a shift in effective index is supposed ($\Delta n_{eff} = 10^{-3}$), a translation in transmittivity spectrum and a change of resonance wavelengths are observed (see Fig. 25)

Assuming the effective index change is due to waveguide cover medium refractive index change, micro resonator sensitivity to waveguide cover medium refractive index changes can be written as:

$$S_r = \frac{\partial\lambda_{res}}{\partial n_c} \tag{41}$$

where $n_c$ is the refractive index of waveguide cover medium. Micro resonator sensitivity depends on waveguide sensitivity as defined in Eq. (17). In fact Eq. (41) can be rewritten in the following form:

$$S_r = \frac{\partial\lambda_{res}}{\partial n_{eff}} \cdot \frac{\partial n_{eff}}{\partial n_c} = \frac{\partial\lambda_{res}}{\partial n_{eff}} \cdot S_w \tag{42}$$

where $S_w$ is the waveguide sensitivity.

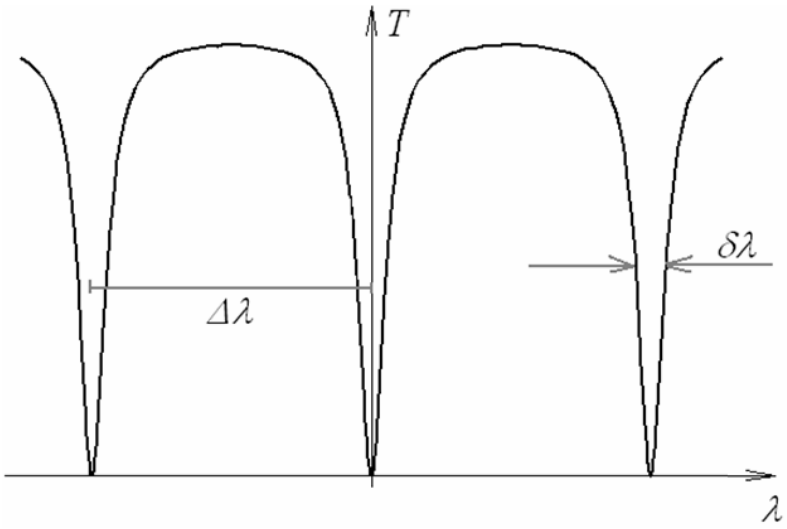


**Figure 24.** Typical transmittivity spectrum of a micro resonator.

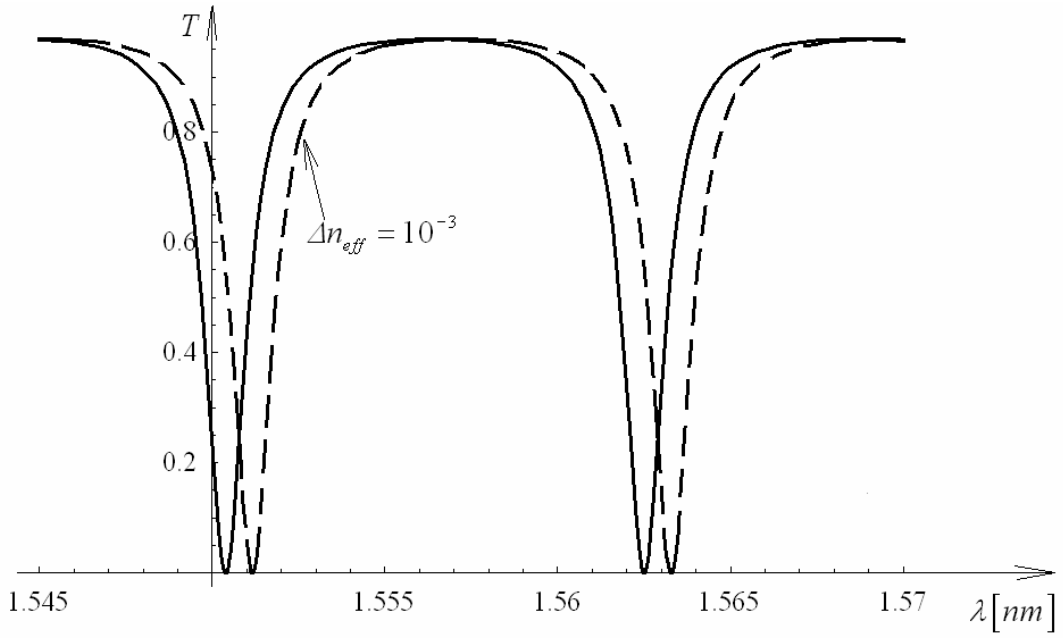


**Figure 25.** Transmittivity spectrum of a micro resonator having $L_t$ = 100 μm, $A$=0.99, $r^2$=0.7, $t^2$=0.3 and $n_{eff}$= 2 and spectrum translation due to a shift in effective index equal to $10^{-3}$.

Using Eq. (38) to calculate the derivative of resonance wavelength with respect to the effective index, we can write:

$$S_r = \frac{L}{q} \cdot S_w . \tag{43}$$

Resonance order $q$ can be estimated as:

$$q \cong \frac{n_{eff}^0 L}{\lambda_{res}^0} \tag{44}$$

where $n_{eff}^0$ is effective index unperturbed value and $\lambda_{res}^0$ is resonance wavelength unperturbed value. Substituting Eq. (44) into Eq. (43), micro resonator sensitivity can be expressed as:

$$S_r = \frac{\lambda_{res}^0}{n_{eff}^0} \cdot S_w . \tag{45}$$

Performance of integrated optical sensors based on micro resonators depends not only on $S_r$, but also on minimum detectable change in resonance wavelength. This quantity depends on $\delta\lambda$ and usually it is equal to $\delta\lambda/10$ [39].

The capability of a microring resonator in SOI technology adopting a Si-wire waveguide and having a radius of 3 μm to sense ammonia concentration changes has been theoretically demonstrated in [40], whereas a design strategy to optimize $Si_3N_4/SiO_2$ microring-based integrated optical sensors has been proposed in [41].

A micro race-track resonator, fabricated using polymeric materials, in which the resonance slope has been enhanced by the introduction of two partially reflecting element (Fig. 26), has been adopted for biochemical sensing (glucose concentration measurements have been performed) [42]. Exploited configuration produces a Fano-resonant line shape that greatly enhances the device sensitivity. Proposed sensor exhibits a minimum detectable concentration change of glucose solution around 0.024%, or 24 mg/dl.

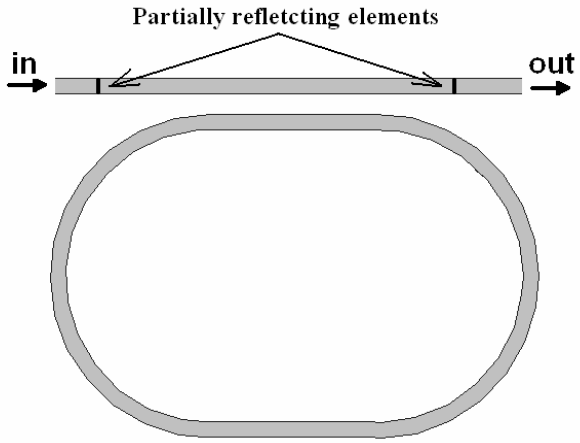


**Figure 26.** Micro racetrack resonator biosensor with sensitivity enhanced by introducing two partially reflecting elements.

A lowering of detection limit related to glucose concentration measurement is obtainable by increasing the micro cavity quality factor *Q*. *Q* value around 20,000 has been estimated for the microring resonator proposed in [43] (fabricated using polymeric materials), so this sensor exhibits a detection limit equal to 0.915 mg/dl in glucose concentration measurement (homogeneous sensing) and equal to 250 pg/mm$^2$ in spavidin molecule detection (surface sensing). Finally, the capability of this sensor to detect shifts of propagating mode effective index around $10^{-7}$ has been also proved.

Vertical coupling between straight waveguide and microring resonator is employed in other biosensors, as in [44] (Fig. 27). Microring quality factor is around 12,000 and detection limit, in terms of minimum detectable change in effective index, is equal to $1.8\times10^{-5}$.

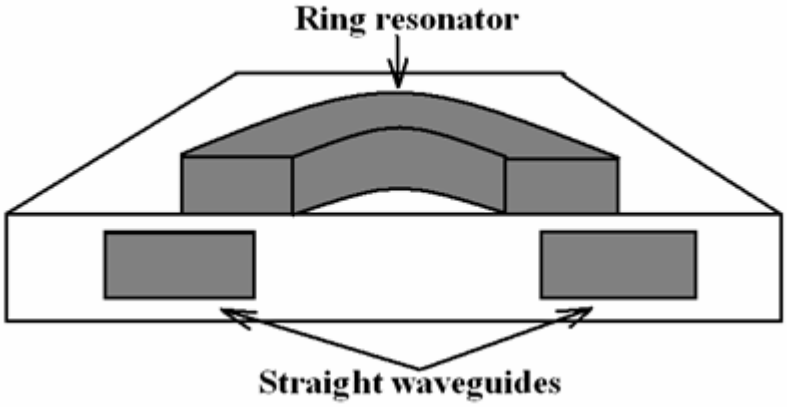


**Figure 27.** Vertical coupling between microring and straight waveguides.

Adopting a $Si_xN_y/SiO_2$ waveguide, a racetrack resonator having a radius of 2 mm has been fabricated for protein detection [45]. This sensor is capable to detect very low concentrations of avidin in phosphate-buffered saline solution (detection limit is equal to 0.1 nM). Adopting a microdisk resonator fabricated using a CMOS-compatible technology ($Si_3N_4/SiO_2$ waveguide) and having a radius of 15 μm, measurement of a change in cover medium refractive index as low as $10^{-4}$ was experimentally demonstrated [46].

## 5. Performance comparison

Table 1 summarizes a comparison in terms of detection limit (expressed as minimum detectable change in cover medium refractive index) and device length among some integrated optical biosensors reported in literature. From this performance comparison, we note that interferometer configurations are usually the most sensitive but they also require very long structures (tens of mm). Photonic sensors based on micro cavities are significantly more compact (a reduction in length of three orders of magnitude is observed) and exhibit a sensitivity which is comparable to that of Mach-Zehnder based sensors. Bragg grating based biosensors is quite compact and very sensitive. Further, their sensitivity can be significantly enhanced adopting sub-micrometer SOI waveguides as guiding structures.

## 6. Conclusions

This paper reviews the wide variety of photonic sensors for biosensing applications proposed in literature, since the fabrication of the first optical biochemical sensor based on the measurement of changes in absorption spectrum and developed for the measurement of $CO_2$ and $O_2$ gas concentration.

Optical technologies allow overcoming some problems connected to use of electrochemical techniques for biosensing analysis as low sensitivity, large dimensions and influence of electromagnetic interference. Biosensing integrated optical architectures enable to reach high sensitivity and selectivity, high compactness and immunity to electromagnetic disturbances. Among these architectures, those realized by CMOS-compatible technologies permit in general to achieve low cost, full technological compatibility between optical sensor and read-out electronics and possibility of mass fabrication. Integrated configurations based on microring and microdisk show very important

advantages related to dimension reduction, without significantly affecting the device sensitivity. Finally, silicon slot waveguides are emerging as a very attractive building block for fabrication of nanometer ultra-sensitive integrated optical biosensors.

**Table 1.** Comparison among integrated optical biosensors.

| Year | Author | Architecture | Technology | Detection limit | Total length [μm] |
|---|---|---|---|---|---|
| 1997 | B. Drapp *et al.* [22] | MZI | Glass | $1.5\times10^{-6}$ | 15,000 |
| 1999 | R.D. Harris *et al.* [30] | SPR | Glass | $1\times10^{-4}$ | 2,000 |
| 2002 | E. Krioukov *et al.* [46] | Disk resonator | CMOS-compatible | $1\times10^{-4}$ | 30 |
| 2003 | F. Prieto *et al.* [21] | MZI | CMOS-compatible | $7\times10^{-6}$ | 30,000 |
| 2003 | A. Ymeti *et al.* [24] | Young | CMOS-compatible | $8.5\times10^{-8}$ | ≈ 50,000 |
| 2003 | F. Prieto *et al.* [28] | MZI (ARROW) | CMOS-compatible | $2\times10^{-5}$ | 15,000 |
| 2004 | S. Campopiano *et al.* [29] | Hollow | CMOS-compatible | $9\times10^{-4}$ | 200,000 |
| 2005 | W. Hopman *et al.* [34] | Bragg grating | CMOS-compatible | $4\times10^{-5}$ | 76 |
| 2006 | F. Dell'Olio *et al.* [40] | Ring resonator | SOI | $1\times10^{-4}$ | 6 |
| 2006 | A. Yalçin *et al.* [44] | Ring resonator | Glass | $1.8\times10^{-5}$ | 120 |

## References


1. Vo-Dinh, T., Allain, L. "Biosensors for Medical Applications", **2003**, in *Biomedical Photonics Handbook*, T. Vo-Dinh, Ed. Boca Raton: CRC Press.
2. Vo-Dinh, T.; Cullum, B. M. "Fluorescence Spectroscopy for Biomedical Diagnostics", **2003**, in *Biomedical Photonics Handbook*, T. Vo-Dinh, Ed. Boca Raton: CRC Press.
3. Vo-Dinh, T.; Tromberg, B. J.; Griffin, G. D.; Ambrose, K. R.; Sepaniak, M. J.; Gardenhire, E. M. "Antibody-based fiberoptics biosensor for the carcinogen benzo(a)pyrene", *Appl. Spectrosc.* **1987**, *41*, 735-738.
4. Vo-Dinh, T.; Nolan, T.; Cheng, Y.E.; Sepaniak, M.J.; Alarie, J.P. "Phase-resolved fiberoptics fluoroimmunosensor", *Appl. Spectrosc.* **1990**, *44*, 128-134.
5. Smith, L. M.; Saunders, J. Z.; Kaiser, R. J.; Hughes, P.; Dodd, C. R.; Cornell, C. R.; Heiner, C.; Kent, S. B. H.; Hood, L. E. "Fluorescence Detection in Automated DNA Sequence Analysis", *Nature*, **1986**, *321*, 674-679.
6. Homola, J.; Yee, S. S.; Gaugliz, G. "Surface plasmon resonance sensors: review", *Sens. Actuators B*, **1999**, *54*, 3-15.
7. Flanagan, M. T.; Pantell, R.H. "Surface plasmon resonance and immunosensors", *Electron. Lett.* **1984**, *20*, 968-970.

8. Mahadevan-Jansen, A. "Raman Spectroscopy: From Benchtop to Bedside", **2003**, in *Biomedical Photonics Handbook*, T. Vo-Dinh, Ed. Boca Raton: CRC Press.
9. Isola, N. R.; Stokes, D. L.; Vo-Dinh, T. "Surface enhanced Raman gene probe for HIV detection", *Anal. Chem.* **1998**, *70*, 1352-1356.
10. Vo-Dinh, T.; Stokes, D. L.; Griffin, G. D.; Volkan, M.; Kim, U. J.; Simon, M. I. "Surface-enhanced Raman scattering (SERS) method and instrumentation for genomics and biomedical analysis", *J. Raman Spectrosc.* **1999**, *30*, 785-793.
11. Yotter, R. A.; Lee, L. A.; Wilson, D. M.; "Sensor technologies for monitoring metabolic activity in single cells – part II: nonoptical methods and applications", *IEEE Sensors Journal*, **2004**, *4*, 395-411.
12. Cerussi, A. E.; Tromberg, B. J. "Photon Migration Spectroscopy Frequency-Domain Tecniques", **2003**, in *Biomedical Photonics Handbook*, T. Vo-Dinh, Ed. Boca Raton: CRC Press.
13. Lillie, J. J.; Thomas, M. A.; Jokerst, N. M.; Ralph, S. E.; Dennis, K. A.; Handerson, C. L.; "Multimode interferometric sensors on silicon optimized for fully integrated complementary-metal-oxide-semiconductor chemical-biological sensor systems", *J. Opt. Soc. Am. B*, **2006**, *23*, 642-651.
14. Luo, D. H.; Levy, R. A.; Hor, Y. F.; Federici, J. F.; Pafchek, R. M. "An integrated photonic sensor for in situ monitoring of hazardous organics", *Sens. Actuators B*, **2003**, *92*, 121-126.
15. Luff, B. J.; Wilkinson, J. S.; Piehler, J.; Hollenbach, U.; Ingenhoff, J.; Fabricius, N. "Integrated optical Mach-Zehnder biosensor", *J. Lightwave Technol.* **1998**, *16*, 583-592.
16. Brosinger, F.; Freimuth, H.; Lacher, M.; Ehrfeld, W.; Gedig, E.; Katerkanp, A.; Spener, F.; Cammann, K. "A label-free affinity sensor with compensation of unspecific protein interaction by a highly sensitive integrated optical Mach-Zehnder interferometer on silicon", *Sens. Actuators B*, **1997**, *44*, 350-355.
17. Weisser, M.; Tovar, G.; Mittler-Neher, S.; Knoll, W.; Brosinger, F.; Freimuth, H.; Lacher, M.; Ehrfeld, W. "Specific bio-recognition reactions observed with an integrated Mach–Zehnder interferometer", *Biosensors & Bioelectronics*, **1999**, *14*, 405-411.
18. Qui, Z.; Matsuda, N.; Itoh, K.; Murabayashi, M.; Lavers, C. R. "A design for improving the sensitivity of a Mach-Zehnder interferometer to chemical and biological measurands", *Sens. Actuators B: Chem.* **2002**, *81*, 254-258.
19. Kerrat, R., Jaffrezic-Renault, N.; Greco, P.; Helmers, H.; Benech, P.; Rimet, R.; "Integrated optical enlarged-field interferometer used as a chemical sensor" *Sens. Actuators B: Chem.***1996**, *37*, 7-11.
20. Maisenholder, B.; Zappe, H. P.; Kunz, R. E.; Riel, P.; Moser, M.; Edlinger, J.; "A GaAs/AlGaAs-based refractometer platform for integrated optical sensing applications" *Sens. Actuators B: Chem.***1997**, *38*, 324-329.
21. Prieto, F.; Sepulveda, B.; Calle, A.; Llobera, A.; Dominguez, C.; Abad, A.; Montoya, A.; Lechuga, L. M.," An integrated optical interferometric nanodevice based on silicon technology for biosensor applications" *Nanotechnol.***2003**, *14*, 907-912.
22. Drapp, B.; Piehler, J.; Brecht, A.; Gauglitz, G.; Luff, B. J.; Wilkinson, J. S.; Ingehoff, J.," Integrated optical Mach-Zehnder interferometers as simazine immunoprobes", *Sens. Actuators B*, **1997**, *38*, 277-282.

23. Qi, Z.; Matsuda, N.; Itoh, K.; Murabayashi, M.; Lavers, C. R.; "A design for improving the sensitivity of a Mach-Zehnder interferometer to chemical and biological measurands", *Sens. Actuators B*, **2002**, *81*, 254-258.
24. Ymeti, A.; Kanger, J. S.; Greve, J.; Lambeck, P. V.; Wijn, R.; Heideman, R. G.," Realization of a multichannel integrated Young interferometer chemical sensor" *Appl. Opt.*2003, **42**, 5649-5660.
25. Prieto, F.; Llobera, A.; Jiménez, D.; Doménguez, C.; Calle, A.; Lechuga, L. M. "Design and Analysis of Silicon Antiresonant Reflecting Optical Waveguides for Evanescent Field Sensor", *J. Lightwave Technol.***2000**, *18*, 966-972.
26. Prieto, F.; Lechuga, L.M.; Calle, A.; Llobera, A.; Domínguez, C. "Optimized Silicon Antiresonant Reflecting Optical Waveguides for Sensing Applications", *J. Lightwave Technol.***2001**, *19*, 75-83.
27. Benaissa, K.; Nathan, A.; "Silicon anti-resonant reflecting optical waveguides for sensor applications", *Sens. Actuators B*, **1998**, *65*, 33-44.
28. Prieto, F.; Sepulveda, B.; Calle, A.; Llobera, A.; Dominguez, C.; Lechuga, L. M. "Integrated Mach-Zehnder interferometer based on ARROW structures for biosensor applications", *Sens. Actuators B*, **2003**, *92*, 151-158.
29. Campopiano, S.; Bernini, R.; Zeni, L.; Sarro, P. M.; "Microfluidic sensor based on integrated optical hollow waveguides", *Opt. Lett.***2004**, *29*, 1894-1896.
30. Harris, R. D.; Luff, B. J.; Wilkinson, J. S.; Piehler, J.; Brecht, A.; Gauglitz, G.; Abuknesha, R. A. "Integrated optical surface plasmon resonance immunoprobe for simazine detection", *Biosensors & Bioelectron.***1999**, *14*, 377-386.
31. Dostalek, J.; Ctyroky, J.; Homola, J.; Brynda, E.; Skalsky, M.; Nekvindova, P.; Spirkova, J.; Skvor, J.; Schrofel, J. "Surface plasmon resonance biosensor based on integrated optical waveguide", *Sens. Actuators B*, **2001**, *76*, 8-12.
32. Homola, J.; Koudela, I.; Yee, S. S. "Surface plasmon resonance sensors based on diffraction gratings and prism couplers: sensitivity comparison", *Sens. Actuators B*, **1999**, *54*, 16-24.
33. Veldhuis, G.J.; Berends, J.H.; Heideman, R.G.; Lambeck, P.V. "An integrated optical Bragg reflector used as a chemo-optical sensor", *Pure Appl. Opt.* **1998**, *7*, L23-L26.
34. Hopman, W. C. L.; Pottier, P.; Yudistira, D.; van Lith, J.; Lambeck, P. V.; De La Rue, R. M.; Driessen, A.; Hoekstra, H. J. W. M.; de Ridder, R. M. "Quasi one-dimensional photonic crystal as a compact building-block for refractometric optical sensors", *IEEE J. Sel. Top. in Quantum Electron.***2005**, *11*, 11-16.
35. Densmore, A.; Xu, D.-X.; Waldron, P.; Janz, S.; Cheben, P.; Lapointe, J.; Delâge, A.; Lamontagne, B.; Schmid, J. H.; Post, E.; "A Silicon-on-Insulator Photonic Wire Based Evanescent Field Sensor", *IEEE Photon. Tech. Lett.***2006**, *18*, 2520-2522.
36. Xu, Q.; Almeida, V. R.; Panepucci, R. R.; Lipson, M.; "Experimental demonstration of guiding and confining light in nanometer-size low-refractive-index material", *Opt. Lett.***2004**, *29*, 1626-1628.
37. Dell'Olio, F.; Passaro, V. M. N.; "Optical sensing by optimized silicon slot waveguides", *Optics Express*, **2007**, *15*, 4977-4993.

38. Xia, F.; Sekaric, L.; Vlasov, Y. A.; "Mode conversion losses in silicon-on-insulator photonic wire based racetrack resonators", *Optics Express*, **2006**, *14*, 3872-3886.
39. De Vos, K.; Bertolozzi, I.; Bienstman, P.; Baets, R.; Schacht, E.; "Optical Biosensor based on Silicon-on-Insulator Microring Resonators for Specific Protein Binding Detection", *Proc. of Symposium IEEE/LEOS Benelux Chapter*, **2006**, 213-216.
40. Dell'Olio, F.; Passaro, V. M. N.; "Ammonia optical sensor based on microring resonator", *Proc. of 11th International Meeting on Chemical Sensors*, **2006**, 27.
41. Dell'Olio, F.; Passaro, V. M. N.; De Leonardis, F. "Surface Sensitivity Optimization of a Microring Resonator for Biochemical Sensing", *Int. Conf. on Tran. Opt. Net. (ICTON) Proc.* Nottingham, 18-22 June, **2006**, *4*, 128-131.
42. Chao, C.-Y.; Guo, L. J. "Biochemical sensors based on polymer microrings with sharp asymmetrical resonance", *Appl. Phys. Lett.* **2003**, *83*, 1527-1529.
43. Chao, C.-Y.; Fung, W.; Guo, L. J. "Polymer microring resonators for Biochemical Sensing Applications", *IEEE J. Sel. Top. in Quantum Electron*.**2006**, *12*, 134-142.
44. Yalçin, A.; Popat, K. C.; Aldridge, J. C.; Desai, T. A.; Hryniewicz, J.; Chbouki, N.; Little, B. E.; King, O.; Van, V.; Chu, S.; Gill, D.; Anthes-Washburn, M.; Selim Unlu, M.; Goldberg, B. B. "Optical sensing of biomelecules using microring resonators", *IEEE J. Sel. Top. in Quantum Electron*.**2006,** *12*, 148-155.
45. Ksendzov, A.; Lin, Y. "Integrated optics ring-resonator sensors for protein detection", *Opt. Lett.* **2005**, *30*, 3344-3346.
46. Krioukov, E.; Klunder, D. J. W.; Driessen, A.; Greve, J.; Otto, C. "Sensor based on an integrated optical cavity", *Opt. Lett.***2002**, *27*, 512-514.

© 2007 by MDPI (http://www.mdpi.org). Reproduction is permitted for noncommercial purposes.